

SANDIA REPORT

SAND97-2725 • UC-705

Unlimited Release

Printed December 1997

Numerical Simulations of Annular Wire-Array Z-Pinches in (x,y) , (r,θ) , and (r, z) Geometries

B. M. Marder, T. W. L. Sanford, G. O. Allshouse

Prepared by

Sandia National Laboratories

Albuquerque, New Mexico 87185 and Livermore, California 94550

Sandia is a multiprogram laboratory operated by Sandia Corporation, a Lockheed Martin Company, for the United States Department of Energy under Contract DE-AC04-94AL85000.

Approved for public release; further dissemination unlimited.



Sandia National Laboratories

Issued by Sandia National Laboratories, operated for the United States Department of Energy by Sandia Corporation.

NOTICE: This report was prepared as an account of work sponsored by an agency of the United States Government. Neither the United States Government nor any agency thereof, nor any of their employees, nor any of their contractors, subcontractors, or their employees, makes any warranty, express or implied, or assumes any legal liability or responsibility for the accuracy, completeness, or usefulness of any information, apparatus, product, or process disclosed, or represents that its use would not infringe privately owned rights. Reference herein to any specific commercial product, process, or service by trade name, trademark, manufacturer, or otherwise, does not necessarily constitute or imply its endorsement, recommendation, or favoring by the United States Government, any agency thereof, or any of their contractors or subcontractors. The views and opinions expressed herein do not necessarily state or reflect those of the United States Government, any agency thereof, or any of their contractors.

Printed in the United States of America. This report has been reproduced directly from the best available copy.

Available to DOE and DOE contractors from
Office of Scientific and Technical Information
P.O. Box 62
Oak Ridge, TN 37831

Prices available from (615) 576-8401, FTS 626-8401

Available to the public from
National Technical Information Service
U.S. Department of Commerce
5285 Port Royal Rd
Springfield, VA 22161

NTIS price codes
Printed copy: A04
Microfiche copy: A01

SAND-97-2725
Unlimited Release
Printed December 1997

Distribution
Category UC-705

Numerical simulations of annular wire-array z-pinches in (x,y), (r,θ), and (r,z) geometries

B.M. Marder, T.W.L. Sanford, G.O. Allshouse
Sandia National Laboratories
P.O. Box 5800
Albuquerque, NM 87185-1110

ABSTRACT

The Total Immersion PIC (TIP) code has been used in several two-dimensional geometries to understand better the measured dynamics of annular, aluminum wire-array z-pinches. The areas investigated include the formation of the plasma sheath from current-induced individual wire explosions, the effects of wire number and symmetry on the implosion dynamics, and the dependence of the Rayleigh-Taylor instability growth on initial sheath thickness. A qualitative change in the dynamics with increasing wire number was observed, corresponding to a transition between a z-pinch composed of non-merging, self-pinching individual wires, and one characterized by the rapid formation and subsequent implosion of a continuous plasma sheath. A sharp increase in radiated power with increasing wire number has been observed experimentally near this calculated transition. Although two-dimensional codes have correctly simulated observed power pulse durations, there are indications that three dimensional effects are important in understanding the actual mechanism by which these pulse lengths are produced.

ACKNOWLEDGEMENTS

We wish to thank R.B. Spielman and M.K. Matzen for vigorous programmatic support; D. Mosher, D.L. Peterson and J.H. Hammer for useful discussions; and M.K. Matzen for carefully reviewing this report.

Contents

1. Introduction	1
2. One dimensional benchmark	1
3. Sheath formation with the (r,θ) code	3
4. Behavior in the (x,y) plane	7
5. The Rayleigh-Taylor instability	11
6. Symmetry breaking.	14
7. Conclusions	17
A personal note	18
Appendix	18
References	20

Figures

1. 1-D pinch simulations.	2
2. Lasnex simulations of individual wire expansions.	3
3. Snapshots of plasma during sheath formation and implosion.	4
4. Average sheath thickness for 10, 20, 40, and 120 wires.	5
5. Azimuthal variation of the sheath for 10, 20, 40, and 120 wires	6
6. Mass and current density for 20 wires at 1, 12, 24, and 29 ns.	7
7. Vector potential, A_z , showing 10 wire and 8 post locations.	8
8. Implosions for 10 wire, 20 wire, and uniform sheaths.	9
9. Radius, Current, and Voltage for the 10 wire pinch.	10
10. Radiation pulse for 10 wires, 20 wires, and uniform shell.	10
11. RT growth for an initial sheath FWHM of 1, 1/3, 3 mm.	11
12. Time dependence of sheath thickness for different initial thickness.	12
13. Involved mass for different initial sheath thickness.	12
14. Pinch with $m=0$ instability numerically removed.	14
15. Imploding pinch with 2mm offset.	15
16. The 20 wire pinch with one wire missing.	15
17. A 20 wire pinch with wires randomly displaced	16
18. Power pulses from the asymmetric (x,y) simulations.	17
19. Radius versus time for equivalent runs in different geometries.	19

1. Introduction.

The Total Immersion PIC (TIP) code has been used in several geometries to understand better the measured dynamics of annular, aluminum wire-array z-pinches [1,2] on the Saturn [3] accelerator. The areas investigated include the formation of the plasma sheath from current-induced individual wire explosions, the effects of wire number and symmetry on the implosion dynamics, and the dependence on wire number of the Rayleigh-Taylor (RT) instability growth. An attempt is made to assess the sensitivity of the radiation pulse duration to phenomena occurring in the various geometries.

TIP, described briefly in the appendix, is a particle-in-cell MHD code with heat conduction, Planckian radiation production and diffusion, and a current equation which couples the plasma to an external circuit. Versions exist in three 2-D geometries: (x,y) , (r,z) and (r,θ) . TIP is a "table top" code which is easy to modify, robust, and quick to run, but whose radiation, equation of state, and opacity models are relatively simple. For this reason, the examples presented here should be interpreted as qualitative guides to possible pinch behavior rather than exact numerical predictions of experimental data.

2. One dimensional benchmark.

A one dimensional z-pinch simulation, depending only on the radius and time, is presented as a benchmark. The parameters, used here and throughout the report, are:

Pinch length: 2 cm

Wire mass: 615 μg of aluminum

Initial annular wire radius: 8.75 mm

Radius of the eight current-return posts: 16.5 mm

External circuit parameters: $L = 10.4 \text{ nH}$, $R = 1/6 \Omega$.

The initial sheath profile is a Gaussian with a millimeter FWHM. The series circuit consists of a voltage source (tabular Saturn voltage as a function of time), an external resistor and inductor, and a plasma load [4].

Figs. 1a and 1b show the time history of the one-dimensional pinch. The radiation plays a small role until near peak compression when it becomes the means by which the plasma sheds the internal energy produced by stagnation, compression, and Joule heating. Several bounces are observed, but these are small and damp rapidly. Figure 1b gives the energy budget. There is a rapid ($\sim 0.1 \text{ nsec}$) rise of the radiation pulse as the thin sheath ($< 0.1 \text{ mm}$ thick) stagnates on axis at speeds of roughly $100 \text{ cm}/\mu\text{sec}$. This enormous, power ($\sim 2500 \text{ TW}$!) is nonphysical, but is typical of 1-D simulations. If the radiation production is artificially turned off, the pinch retains enough thermal energy to rebound and undergo a more leisurely re-compression, as in Fig. 1c.

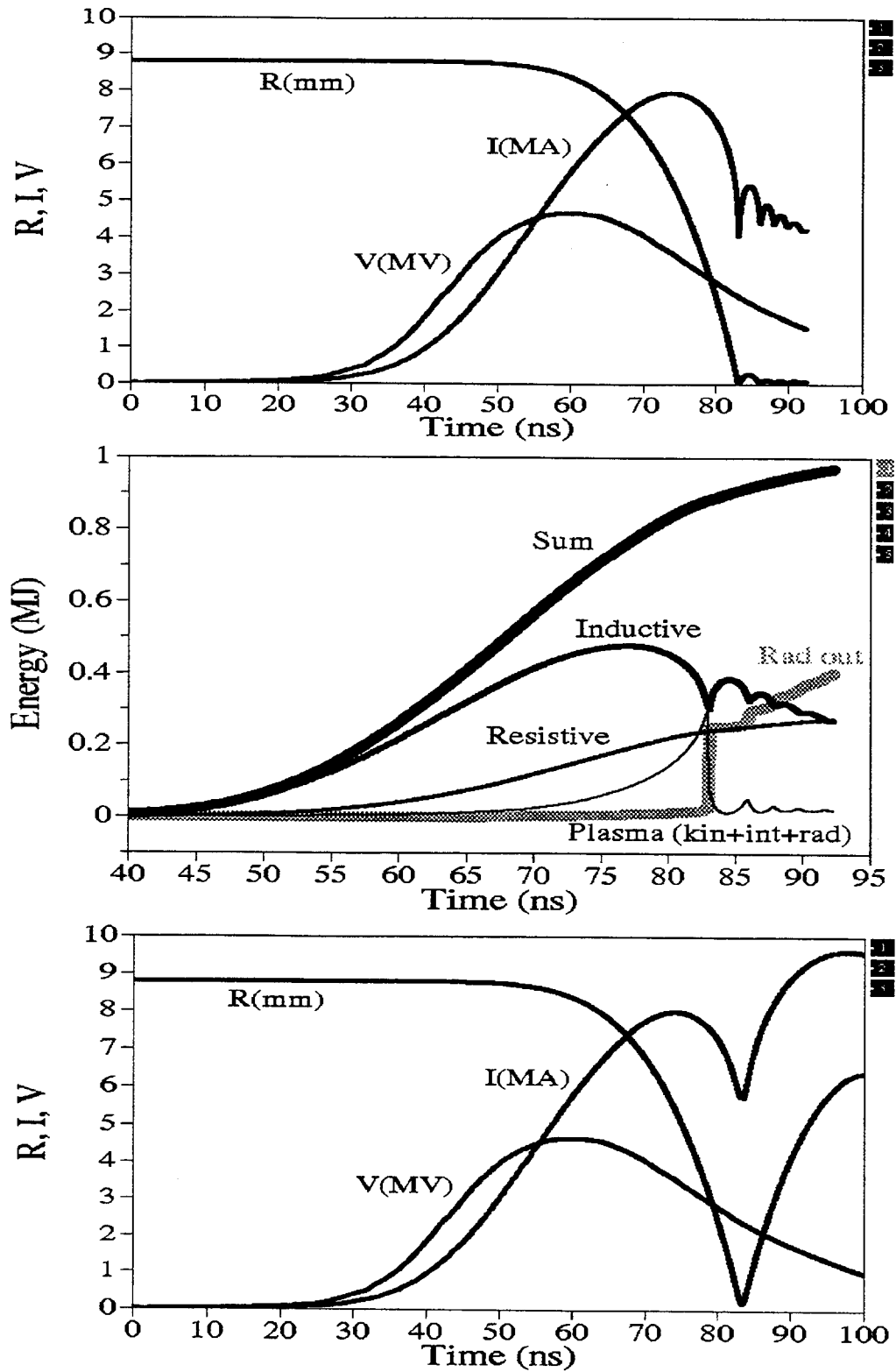


Figure 1. a) 1-D Radius, Current, Voltage. b) Energy: Inductive (plasma+vacuum magnetic and external inductance), resistive (external resistor), plasma (internal+kinetic+trapped radiation), radiated. c) Radius, Current, Voltage, no radiation.

3. Sheath formation with the (r,θ) code.

The pinch begins with the current-induced explosion of an annular multiple wire array. Single wire behavior, shown in Fig. 2, is modeled with 1-D Lasnex to take the wires from their cold, solid state to an expanding plasma, at which time TIP is used to begin simulating the multiple wire array. The current is approximated by a linearly rising prepulse similar to that measured [1], which begins at -100 ns and rises to 100 kA at $t=35$, at which time the full Saturn current has begun to rise. Four cases are considered: 10, 20, 40, and 120 wires with the initial parameters given above. The wire diameter is adjusted to give equal total mass and the appropriate fraction of the total current flows through each wire. The individual wire expansion is followed with Lasnex until its outer edge is half the distance to its neighbor. For example, with an 17.5 mm diameter, the array circumference is about 55 mm. For 20 wires, this gives an inter-wire spacing of 2.75 mm. The TIP simulation for this case begins when the individual wire diameter is half that, or 1.375 mm. This defines the initial time and current, along with radial density, temperature, and velocity profiles from Lasnex, for the (r,θ) TIP simulations. Periodic boundary conditions in theta are imposed.

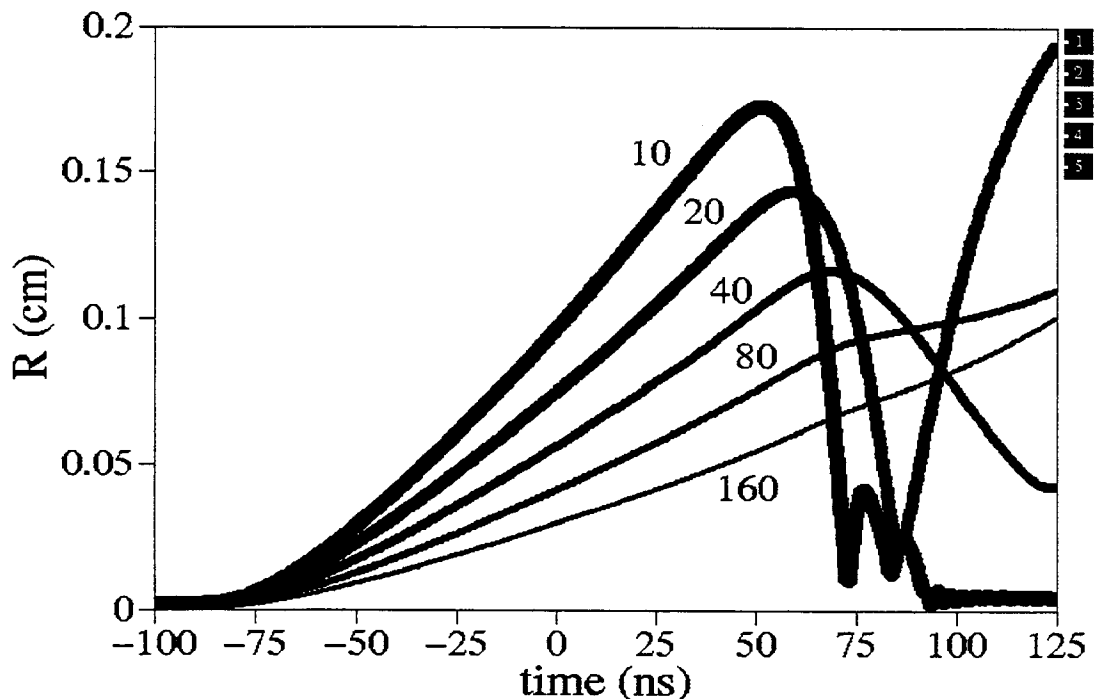
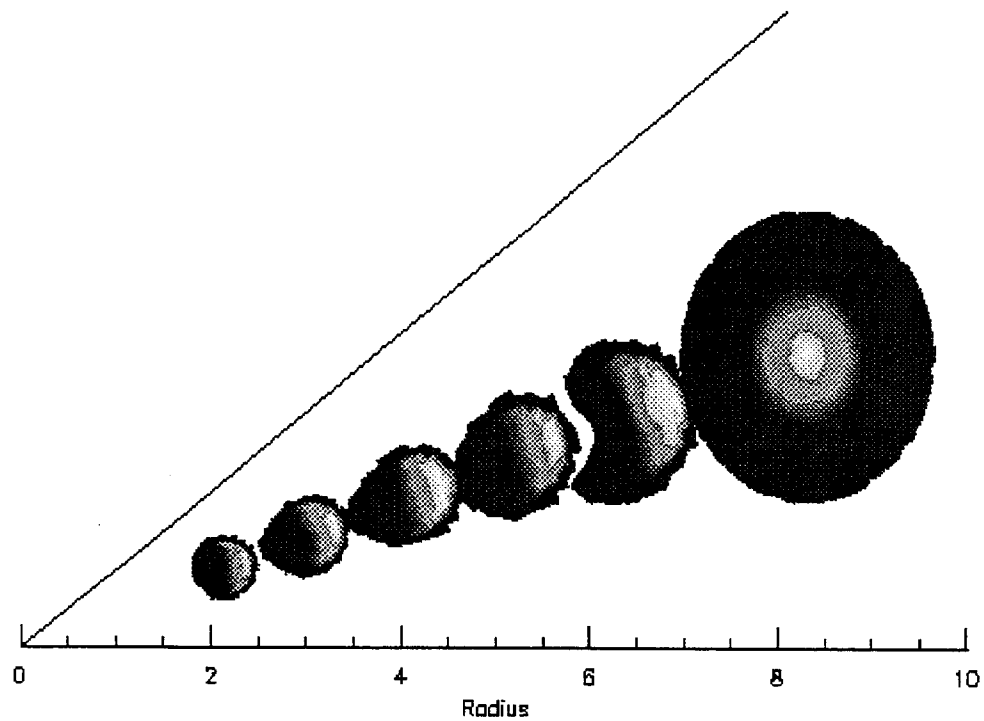


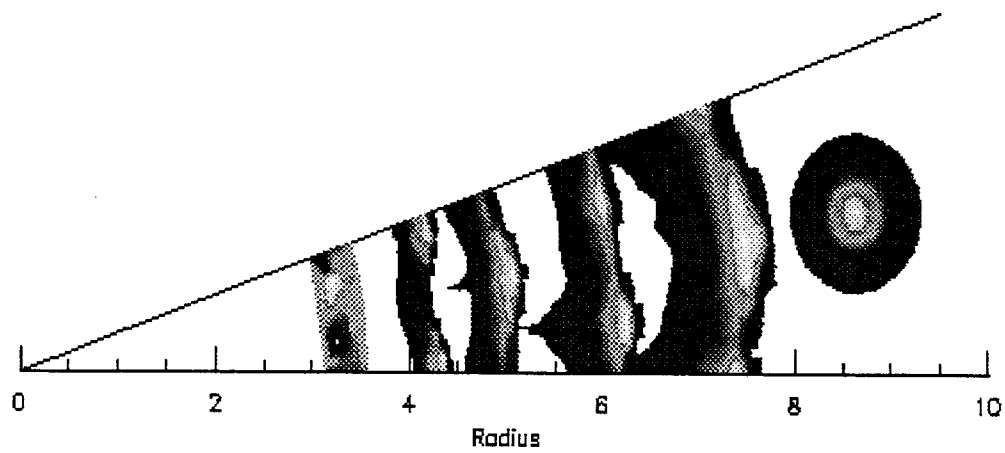
Figure 2. Lasnex simulations of individual wire expansions corresponding to pinches with indicated number of wires.

The wire merging and sheath formation is illustrated in Fig. 3 for three of the four cases. In the 10 wire simulation, the individual self-pinching remains sufficiently vigorous that the wires never merge into a continuous sheath. When a sheath does form in the 20, 40, and 120 (not illustrated) wire cases, there is considerable azimuthal “sloshing” of the density. Because the plasma viscosity is low (water “sloshes” whereas viscous honey “settles”), these density standing waves persist well into the compression. Periodicity in θ is imposed.

10 wires, 36°



20 wires, 18°



40 wires, 9°

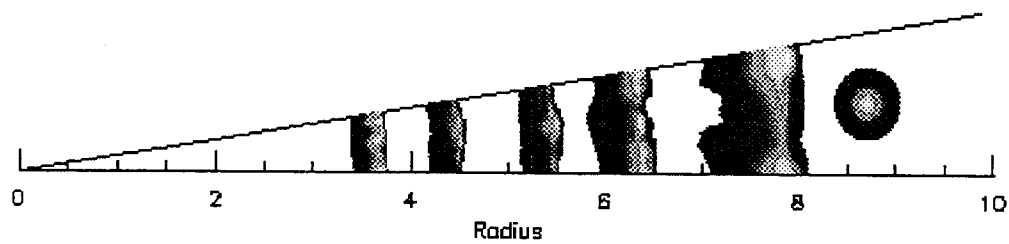


Figure 3. Snapshots of plasma during sheath formation and implosion for 10, 20, and 40 wires.

A time history of the average sheath thickness (FWHM) in the radial direction is given in Fig. 4. The thickness of the imploding sheath is seen to depend inversely on the number of wires before about 75 ns. The thinnest sheath belongs to the 120 wire case, the thickest to the 10 wire case, although this has not actually formed into a continuous sheath. After 75 ns, when the sheath has reached 5 mm (see Fig. 1a), this difference has all but vanished and all sheaths are about 0.1 mm thick and decreasing.

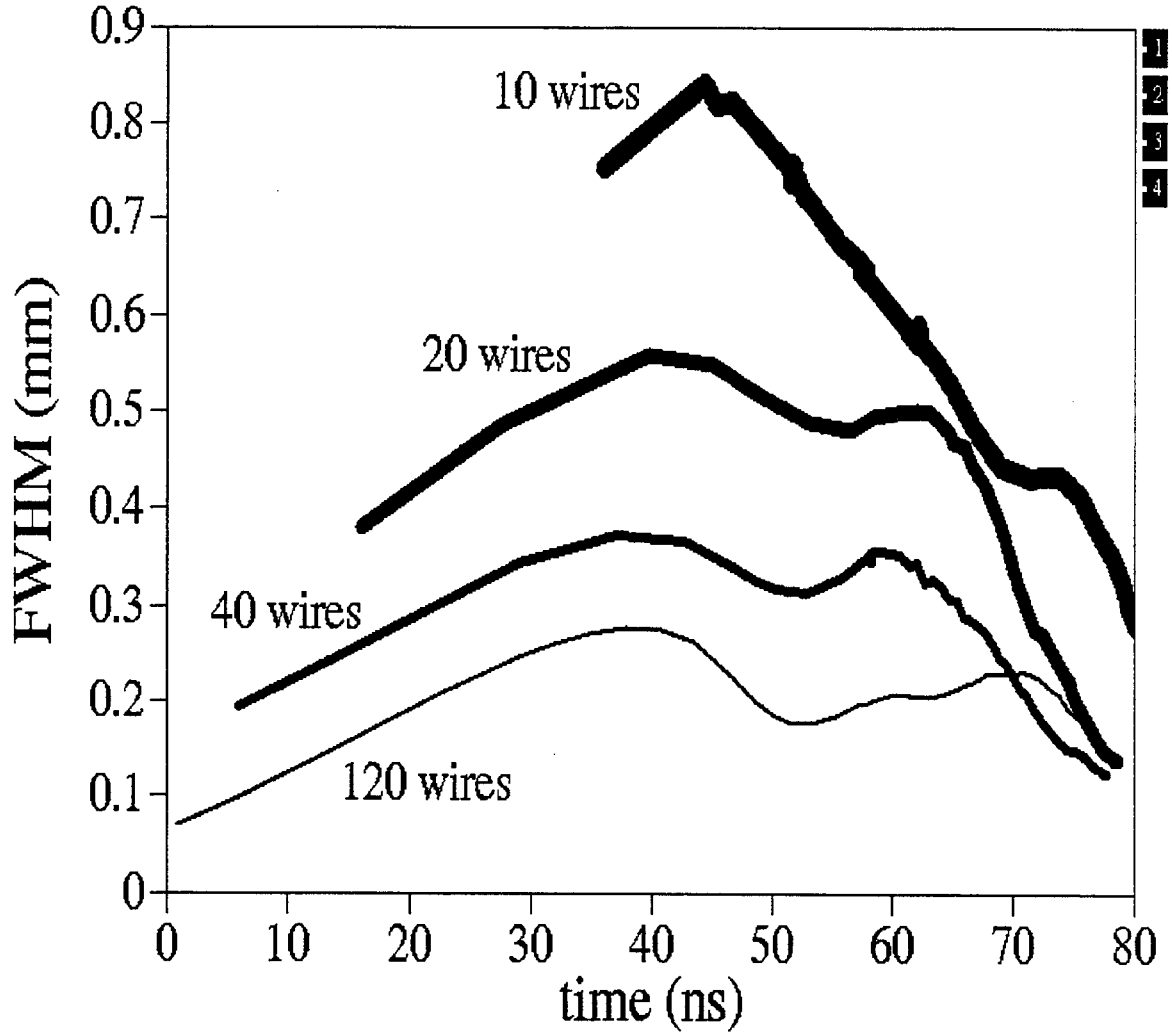


Figure 4. Average sheath thickness (FWHM) for 10, 20, 40, and 120 wires.

A mass-weighted measure of the azimuthal density variation of the sheath, w , is defined by

$$(1) \quad w = \frac{\sum_L |\overline{\rho(L)} - \rho_{av}|}{\rho_{av} L_{MAX}}, \quad \text{where } \overline{\rho(L)} = \frac{\sum_M \rho(L, M)^2 \text{Vol}(L, M)}{\sum_M \rho(L, M) \text{Vol}(L, M)} \quad \text{and} \quad \rho_{av} = \frac{\sum_L \sum_M \rho(L, M)^2 \text{Vol}(L, M)}{\sum_L \sum_M \rho(L, M) \text{Vol}(L, M)}.$$

These definitions eliminate the vacuum, $\rho=0$, from the computation. A plot of w is shown in Fig. 5. The numerical index L corresponds to angle, while M corresponds to radius. $\text{Vol}(L,M)$ is the volume of a numerical grid element. All four cases start with the wire filling roughly half the available space, so their initial variations are equal. The sheath uniformity for the last three cases is seen to approach essentially the same value by about 70 ns. The 10 wire case, since it never does merge, retains the z variation it had initially. The counter-rotating density pulses notwithstanding, the sheaths are seen to achieve a fairly high degree of azimuthal uniformity in all cases.

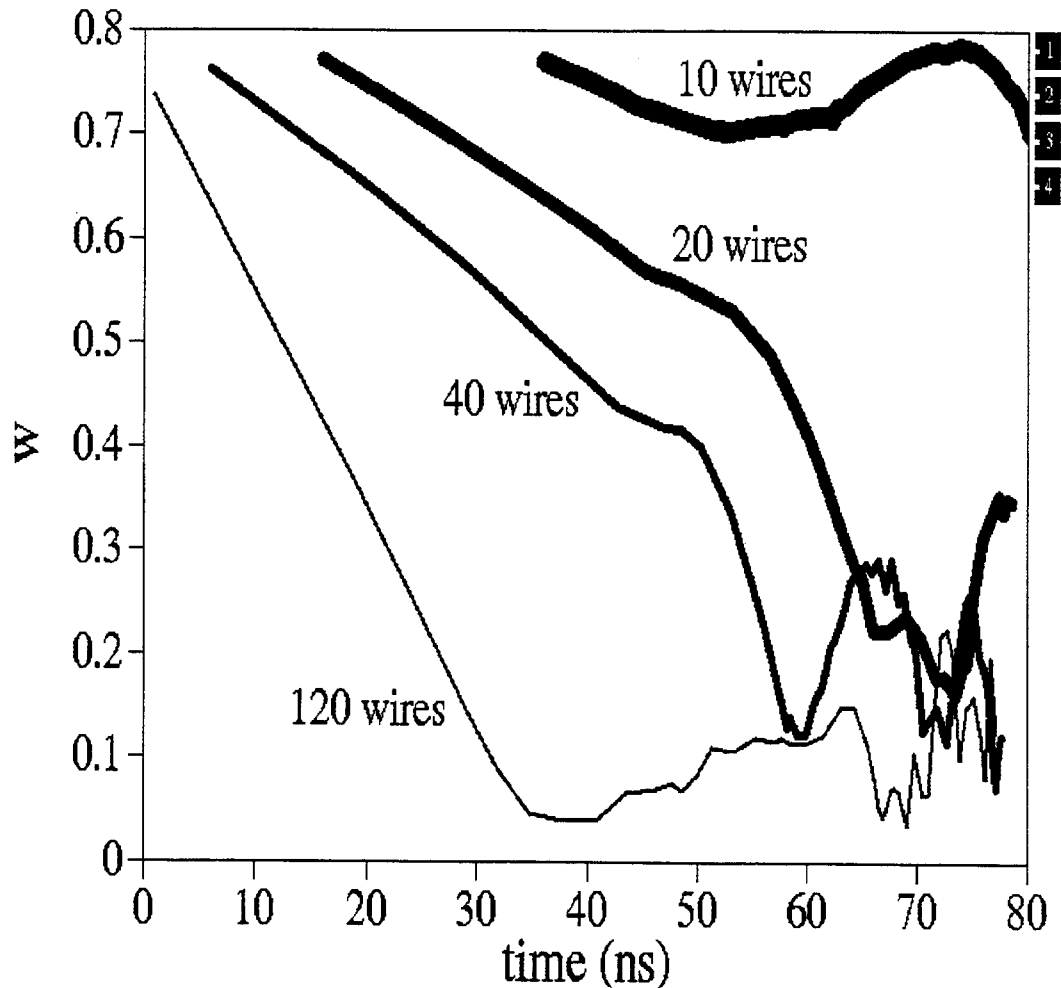


Figure 5. Azimuthal variation W (defined in eq. 1) of the sheath for 10, 20, 40, and 120 wires

Figure 6 shows both the mass density and current density during the merging and sheath formation for the 20 wire case. The initial current density is clearly quite different from the one dimensional approximation in that current flows only on the outer half of the wire. Unlike the 10 wire case, the 20 wires physically merge before the tendency to self-pinch, altered by the one-sided magnetic force, reasserts itself. In this geometry, the field is stronger where the plasma bulges outward so it tends to smooth radial irregularities, quite unlike the growing instabilities which, as will be examined later, are present in (r,z) .

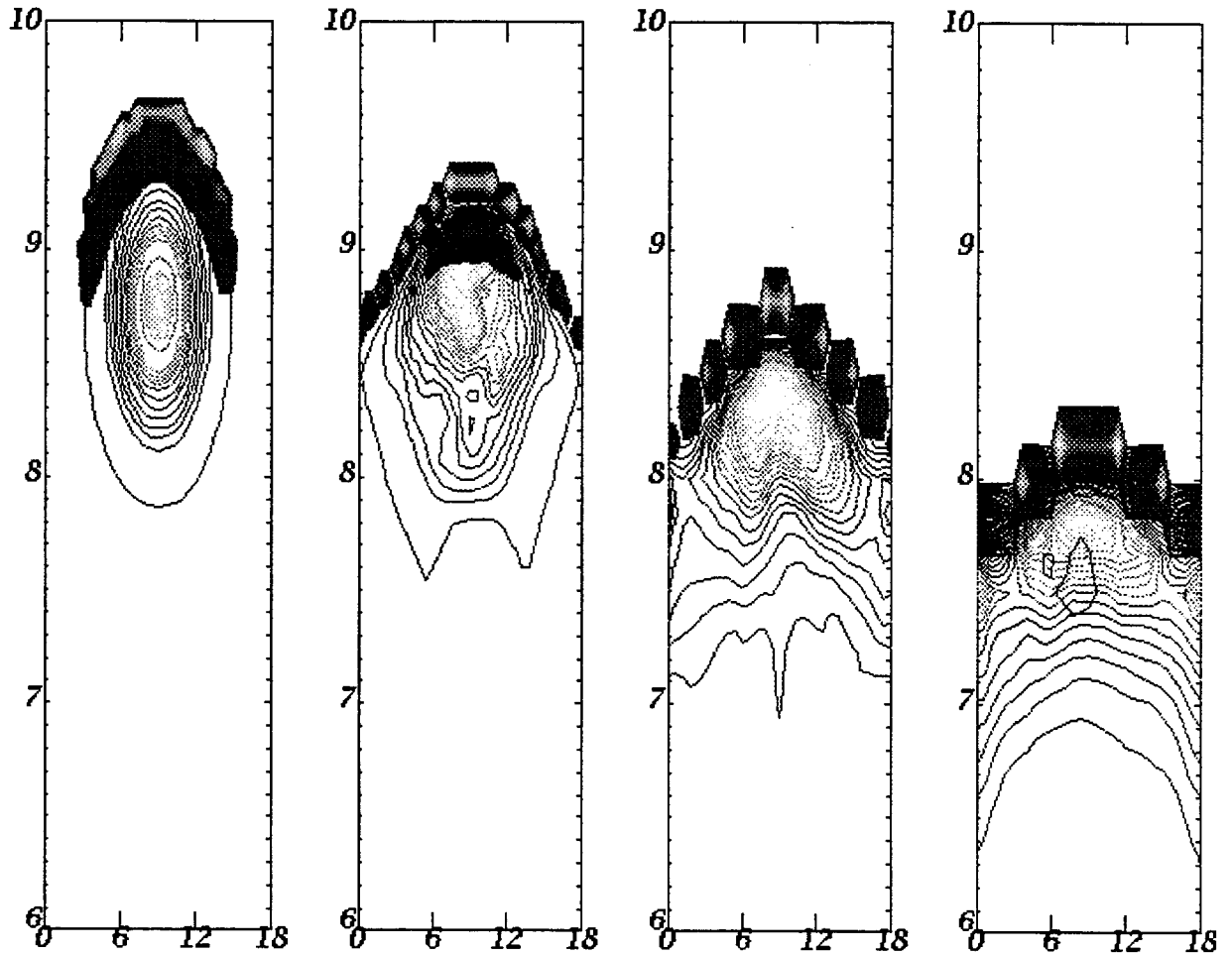


Figure 6. Mass density (line contour) and current density (solid contour) for 20 wires at 1, 12, 24, and 29 ns. The horizontal axis is degrees, the vertical axis is radius in mm.

Two issues which could affect radiation production are raised by these (r,q) simulations. The first is the possible failure to merge into a sheath during the radial compression. The second, because fewer wires produce thicker sheaths, is the effect of the early time sheath thickness on the subsequent development of the RT instability. These issues are now addressed.

4. Behavior in the (x,y) plane.

One of the important early observations from our multiple wire z-pinches was the presence of a sharp increase in the radiated power when the initial inter-wire gap fell below about 1.4 mm, corresponding to about 40 wires [1]. Referring back to Fig. 2, Lasnex simulations indicate that larger diameter wires expand at first but then self-pinch as the current rises. Smaller diameter wires, however, continue their expansion into the large current regime. For the experimentally generated current pulses, the transition occurs at around 40 wires. These simulations, being one dimensional, did not take into account the two dimensional exclusion of the magnetic field from the interior of the wire array and the resultant weakening of the magnetic force on the inside, but they were suggestive of a qualitative change in behavior around this wire number. In the (r,θ) TIP

simulations using Lasnex for initiation, the expansion reversal seen in the 1-D runs was observed with the full wire array, with the caveat that, if the expanding wires physically touched before re-compression, they did not necessarily self-pinch, but rather formed into a sheath.

The wire expansion behavior depends critically on the resistivity. Getting this right through a regime which starts as cold, solid metal wires and ends as a several eV plasma orders of magnitude lower in density, is a challenge. About all one can do is take the best models available and perform a parameter study to determine the sensitivity to questionable parameters. The outcome of just such tests indicate considerable sensitivity to the resistivity in the explosion dynamics. For this reason, the results presented here should be viewed more as qualitative indicators of expected behavior than as precise predictions. For example, the numerical simulations have the wires merging at about 20 wires, rather than the roughly 40 suggested by the experiments. The important conclusion is that this qualitative change in behavior can occur, even if these 2-D simulations fail to predict the exact number of wires at which it happens.

The (x,y) code, rather than the (r,θ) , is used to simulate the entire multiple wire pinches for several reasons. It eliminates the troublesome numerical singularity at the origin which plagues (r,θ) codes. It also allows for a natural treatment of azimuthal asymmetries, which are, in fact, present even in the simplest case. One cause of asymmetry is illustrated in Fig. 7 which shows the early-time magnetic field for a ten wire pinch in which the eight current return posts are visible. Since no current flows at radii less than the wire array, there is no B_θ in the interior.

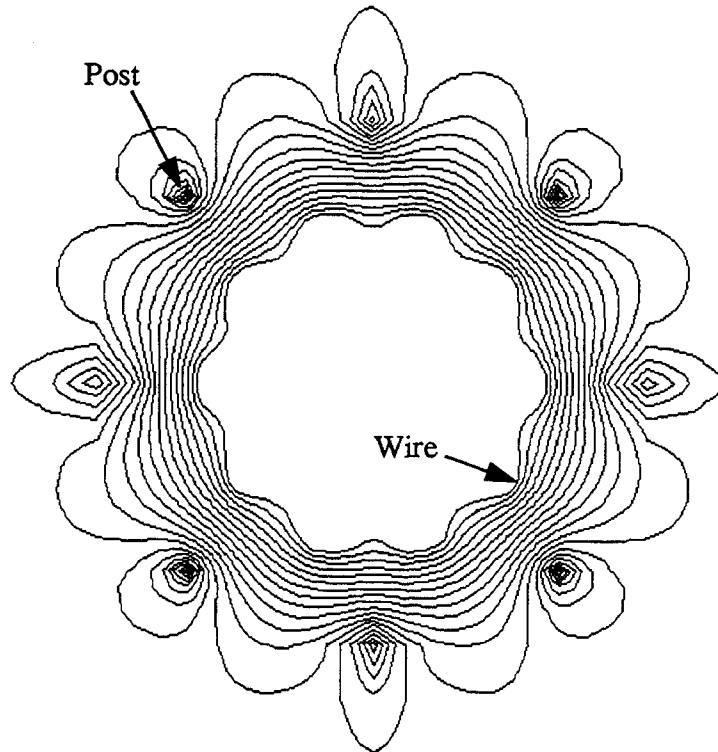


Figure 7. Contours of constant vector potential, A_z , at early times showing 10 wire and 8 post locations. The wire array radius is 8.75 mm; the posts are at 16.5 mm.

Figure 8 shows the time history of 10 and 20 wire pinches, along with a uniform plasma shell. The latter should, and does, reproduce the 1-D behavior of Fig 1a. Unlike the (r,θ) simulations in which 1-D Lasnex runs were used as initial conditions, in these simulations the initial wire configuration is taken simply as a 1mm FWHM Gaussian at 1eV with no initial velocity and no precursor current. Even so, the results are quite similar. As we saw in (r,θ) , single wire simulations are good predictors of behavior even though the field is no longer symmetric. The 10 wires self-pinch sufficiently rapidly that they do not merge until very near the center, while the higher wire numbers form an imploding sheath.

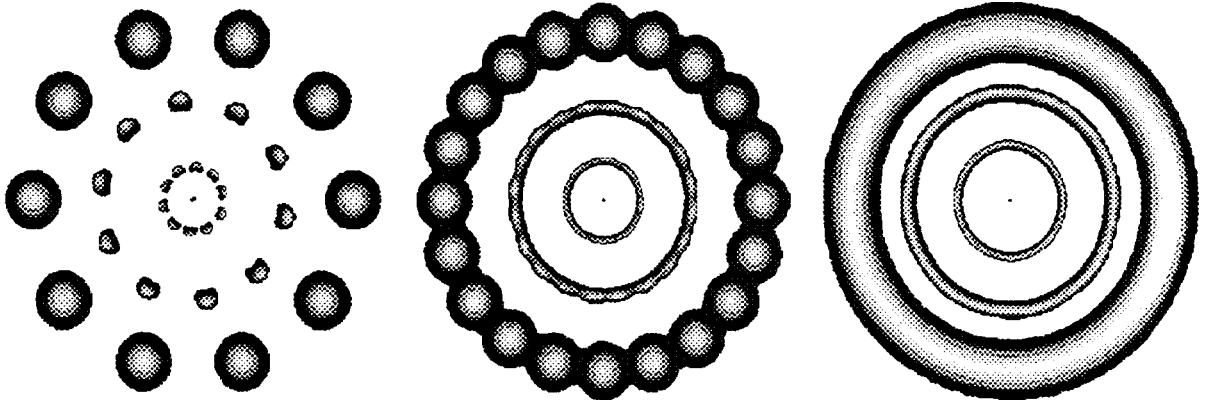


Figure 8. Density contours when the sheath is at 8.75, 5, 2 mm radius and at peak compression for a) 10 wire, b) 20 wire, and c) uniform density shell. Apparent rotation is a numerical artifact. The current-return posts are not shown in this, and subsequent (x,y) plots.

In TIP, all the information resides in the particles. The grid is superimposed at each time step to compute ensemble averages. To eliminate “imprinting” the numerical grid on the physics, the (x,y) mesh is defined each time step at both a random location and with a random angle. This numerical artifact causes the apparent rotation of the wire implosion in Fig. 8.

The actual behavior of the pinch could be strongly affected by RT instabilities in the z direction, so one would not expect it to follow the illustrated behavior throughout the implosion. Nonetheless, these simulations suggest a reason for the observed qualitative change in behavior as the wire number increases past 40. That is, it marks the transition between a convergence of individual, non-merging, wires each of which is undergoing its own mini-pinch, and the implosion of a continuous (at least in its ability to carry current) plasma sheath.

Figure 9 gives the mass-averaged radius, current, and voltage for the 10 wire array. Figure 10 gives the radiation pulse for all three cases. Notice that although more radiation is produced with the more symmetric geometry, the pulse duration is very narrow in all instances, much like the 1-D result. Comparing these with the 1-D simulation, Figs. 1a and b, shows just how little the number of wires affects either the gross dynamics or the radiation pulse duration, at least in the absence of RT instabilities.

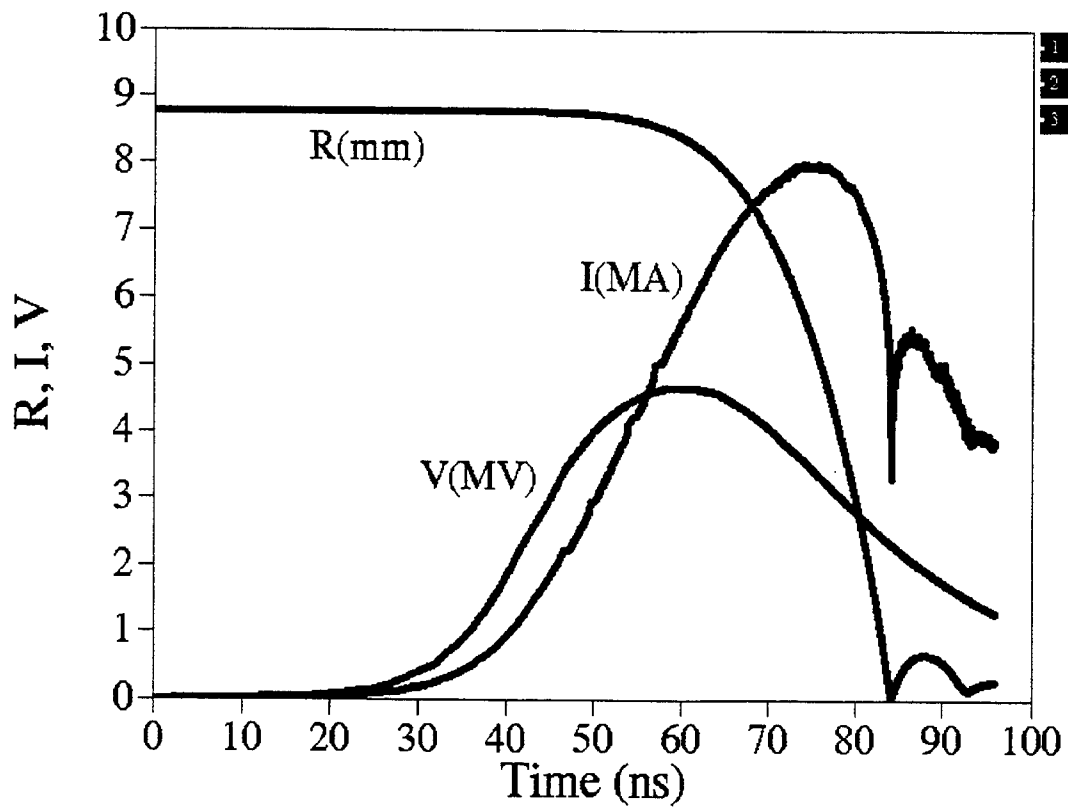


Figure 9. Radius, Current, and Voltage for the 10 wire pinch.

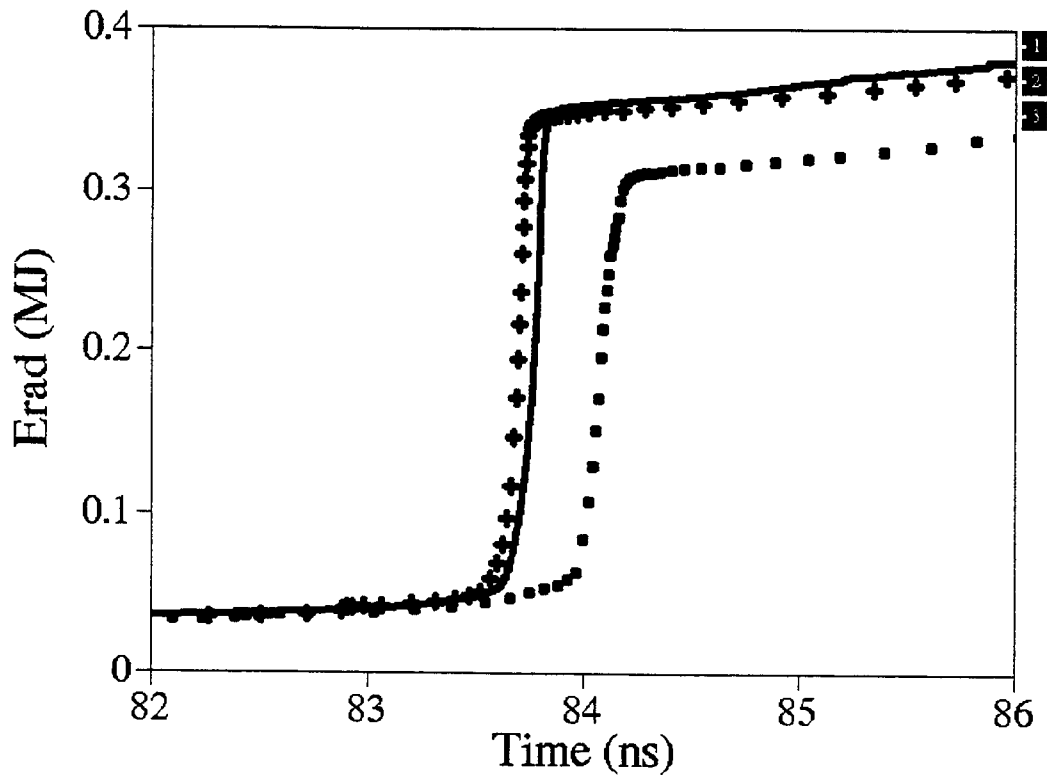


Figure 10. Radiation pulse for 10 wires (square), 20 wires (cross), and uniform shell (solid).

5. The Rayleigh-Taylor Instability.

In this section, RT instability growth is examined using (r,z) TIP. Clearly, unless some initial perturbation is imposed, the behavior will simply reproduce the 1-D results. The perturbation is typically an initial random density variation. With an appropriate choice for the magnitude of this random density perturbation, Jim Hammer [5] showed that the growth of the RT instability, and the resultant increase in the thickness of the plasma sheath at the time of stagnation, can account for the width of the radiation pulse measured for our 90-wire implosions [4]. The dependence of such RT growth on a wide range of initial sheath densities and radii has been studied by Darrell Peterson [6]. His pulse width analysis, keeping the density perturbation fixed, is found to be in excellent agreement with our measured widths in the many-wire, plasma sheath regime [2]. For these TIP runs, a 10% random cell-to-cell density variation is imposed. Only 6 mm of the full 20 mm is simulated and periodic boundary conditions in z are imposed.

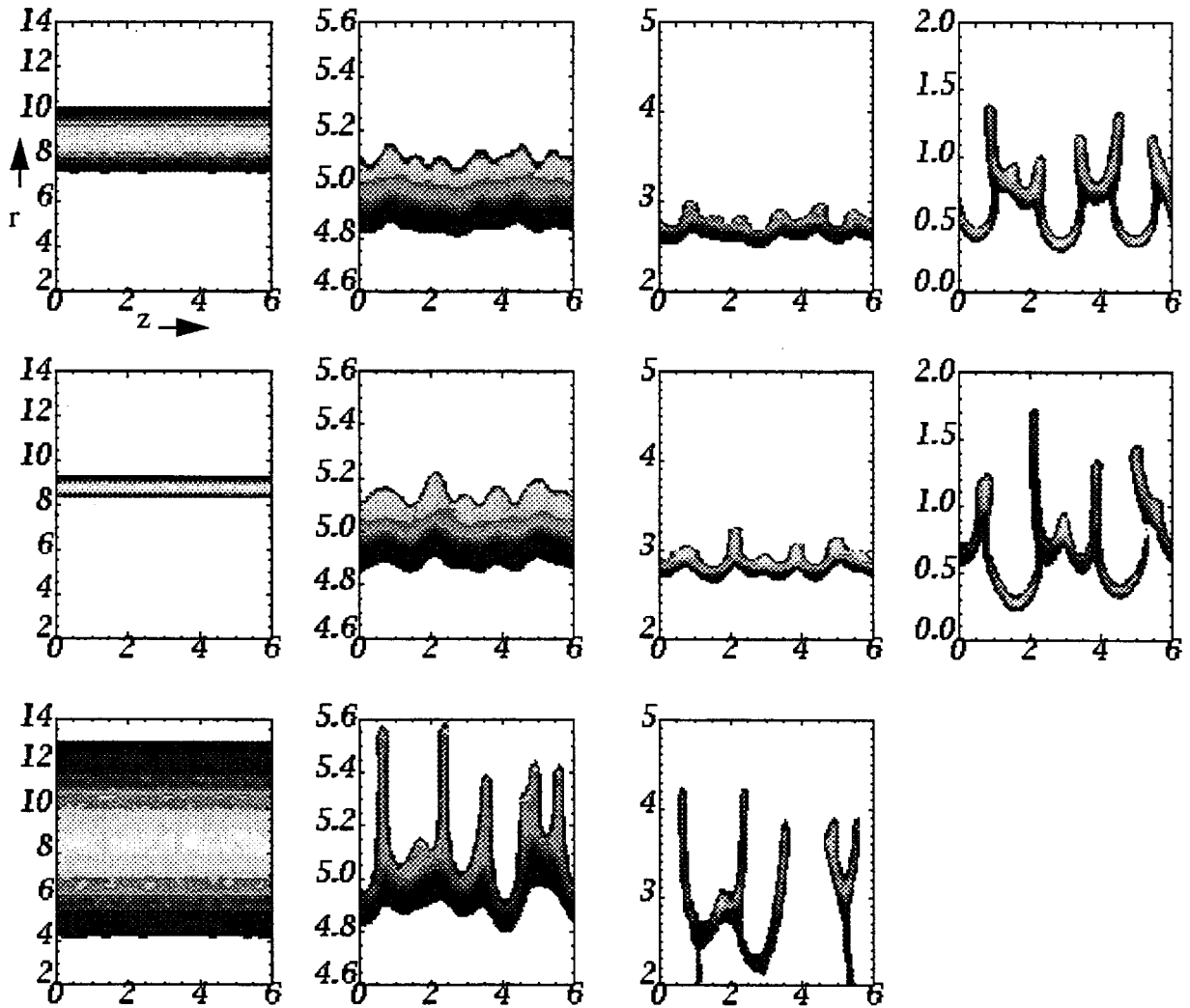


Figure 11. Density contours at average pinch radius of 8.25, 5.0, 3.0, and 0.5 mm showing RT growth for an initial sheath FWHM of (from top) 1, 1/3, 3 mm. The “bubbles” break through after the last frame, cutting the current path. Units are mm.

As discussed in Section 3 (Fig. 4), different wire numbers produce early-time sheaths of differing thickness. To see what effect the sheath thickness has on RT growth, three thicknesses are simulated in (r,z) . Figure 11 shows these simulations. Figure 12 plots the average sheath thickness (FWHM) while Fig. 13 gives Darrell Peterson's "involved mass" [8] for the three cases. Involved mass measures the radial spread in the sheath caused by the growing instability, and is defined analogously to (1) except that the variation is in radius rather than azimuth. As can be seen in these figures, the RT appears somewhat earlier with the very thick sheath, corresponding to fewer wires in the (r,θ) calculation, and then grows at about the same rate, causing the implosion to be disrupted sooner. The pattern, however, does not persist, and may even reverse. For the two thinner sheaths, the RT growth is virtually the same, if anything, growing a bit faster for the very thin sheath.

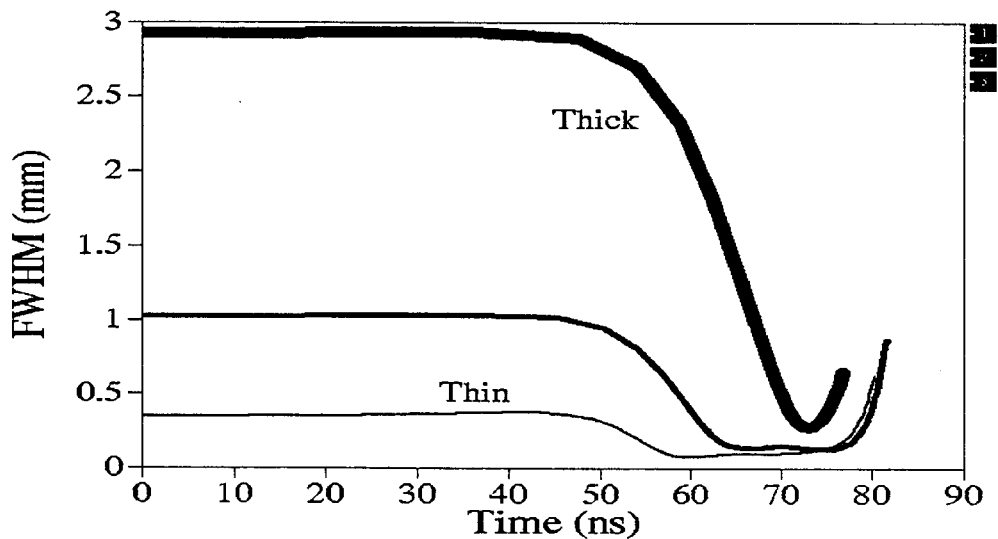


Figure 12. Time dependence of sheath thickness (FWHM) for different initial thickness.

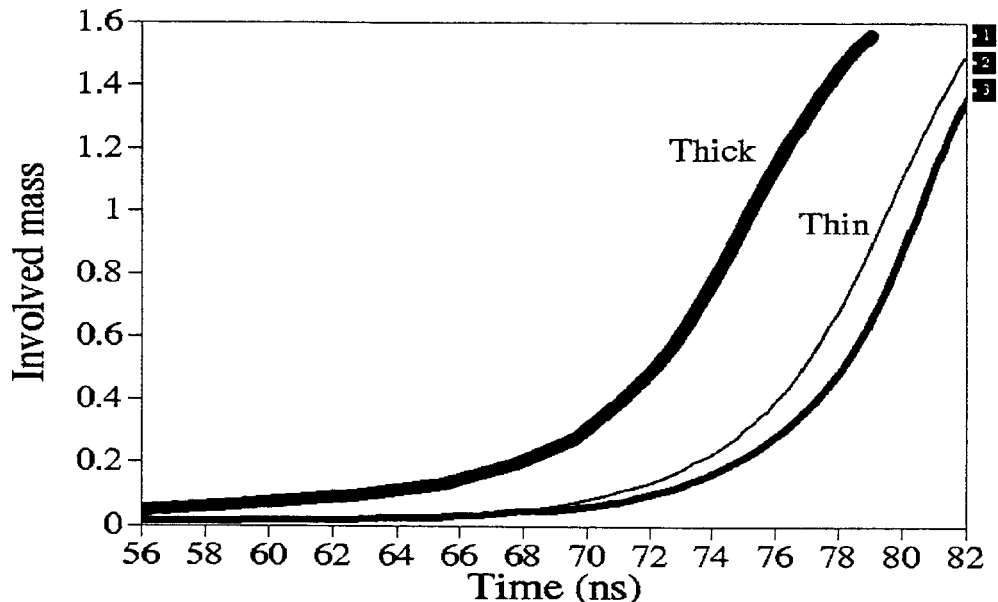


Figure 13. Involved mass for different initial sheath thickness.

What happens when the “bubbles”, those large voids ballooning into the center in Fig. 11, break through to the extent that the current path is interrupted? In TIP, the plasma is represented by numerical fluid “particles” and when the last particle leaves a cell, there is no mechanism by which current can be carried in that cell. In 2-D, no alternate path exists. Since current continues to flow in the experiment, a problem arises as to how this current flow should be handled to allow the simulation to proceed. The situation is rather bizarre in that Spitzer resistivity is a function only of the temperature, being independent of density (what about $\rho=10^{-10}$ or even 0?). One method of overcoming this in 2-D Eulerian codes, in which density is computed from difference equations and is, in general, not identically zero, is by defining a cutoff density for the plasma conductivity [8]. Care must be taken in doing this. If the cutoff is too large, the current path will be broken, as in TIP. If is too small, the “vacuum” conducts virtually everywhere and the current flows along the upper numerical boundary, never influencing the plasma. If, however, it is chosen within acceptable bounds, current can flow across the very low density regions in the bubbles, short circuiting the instability, and allowing the simulation to proceed. It seems plausible that, in reality, the breakthrough of these bubbles indicates the onset of three dimensional behavior in which the current seeks an alternative path at a different azimuth. Other explanations, such as the formation of 2-D ion or electron diodes across bubbles, do not appear to offer viable alternatives. While the 2-D simulations do a good job of reproducing some of the experimentally observed behavior [2], a better understanding of where current actually flows in the experiments probably requires the third dimension.

In the simulations in Fig. 11, the average sheath thickness grows to about 2 mm. If it retains this spread, hits the center near the experimentally observed 50 cm / μ sec, and if radiation is produced as plasma thermalizes on axis, a pulse duration of some 4 ns (2 mm/(0.5 mm/ns)) would be expected. This duration is close to the observed value for our highly symmetric 90-wire shots [4], and is the mechanism believed responsible for the observed pulse width.

The $m=0$, or sausage, instability on the sheath (as opposed to individual wires individual wires), caused by the $1/r$ dependence of the magnetic field, produces behavior similar to the RT. Any radial perturbation on the outer sheath creates a stronger magnetic field at the “valleys” than at the “peaks”, increasing the disturbance. To determine which is most responsible for the bubble and spike development seen in Fig. 11, the growth rates of the two instabilities are compared. The RT growth rate, γ_R , and the $m=0$ growth rate, γ_m , are approximated by

$$(2) \quad \gamma_R = \sqrt{ka} \quad \text{and} \quad \gamma_m = \frac{B}{R\sqrt{\mu\rho}},$$

where k is the RT wave number, B is the magnetic field, R is the average plasma radius, ρ is the average plasma density, and “ a ” is the acceleration given by $J \times B / \rho$. Assuming J flows uniformly in a plasma with sheath thickness “ h ”, their ratio is found to be

$$(3) \quad \frac{\gamma_R}{\gamma_m} = R \sqrt{\frac{k}{h}}.$$

When R is larger than the RT wavelength and h , such as during the implosion, the RT dominates. To see how much the $m=0$ contributes, the vacuum magnetic field, rather than being $\mu I/2\pi r$, is set to $\mu I/2\pi R$. The field has the same average value, but the local $1/r$ dependence is removed, eliminating the $m=0$ instability. This definition of B is used only in the force equation; the actual value is still used to calculate the inductance. Surprisingly, the $m=0$ is found to play almost no role! As seen in Fig. 14, which gives the involved mass for the two cases, the RT instability growth is virtually unaffected by the other instability. The slight difference in the curves is caused by small differences in the overall motion with the numerically altered field definition.

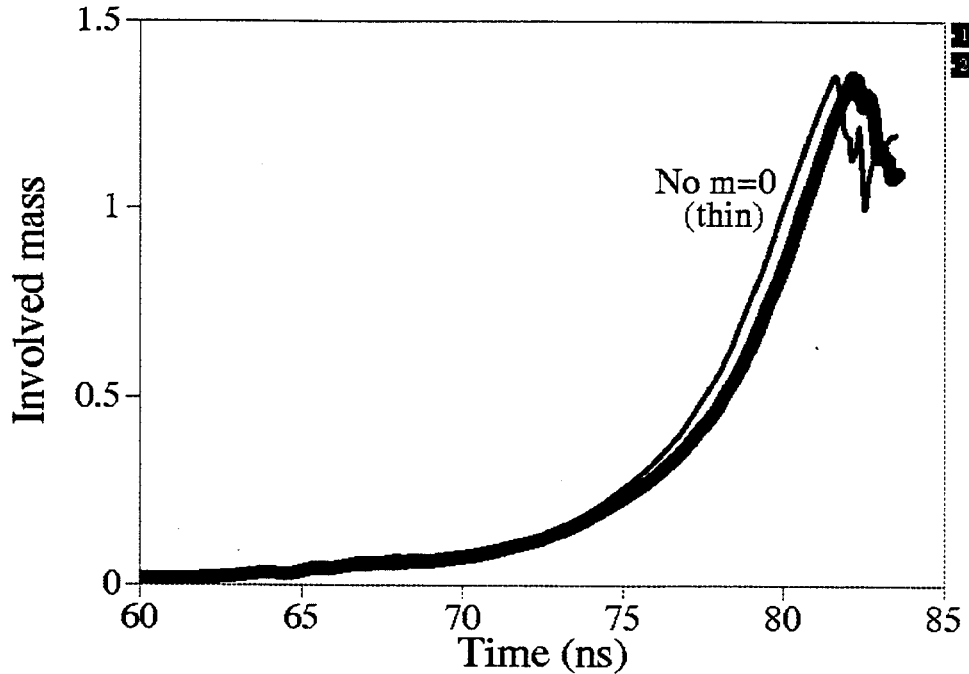


Figure 14. Involved mass, normal (thick) and with $m=0$ instability numerically removed (thin).

6. Symmetry breaking.

There are many ways (other than the eight current-return posts) the symmetry of the wire array pinch can be broken. In this section, the effect of several of these ways on the implosion and subsequent radiation production is examined. The benchmark is the infinite wire implosion illustrated in Fig. 8c. The duration of the radiation pulse is used as a performance metric.

Suppose the initial wire array is offset 2 mm with respect to the current-return posts. Figure 15 shows this case when the imploding sheath has reached a diameter of 4 mm. Notice the evidence of the initial post proximity. Asymmetry can result from a missing wire, as in Fig. 16, where the 20-wire pinch in Fig. 8b has lost one of its members. Because all current-carrying parts attract each other, the sheath acts like a stretched rubber band. When a piece is missing, the sheath circumference opens up as it implodes. Figure 17 shows a 20-wire pinch in which each wire is given the rather sizable random variation in its initial position equal to 10% of its distance to the center. Finally, although not strictly speaking a symmetry breaking, the pinch could have some initial rotation. A simulation was also run of the uniform ring rotating at $0.1 \text{ cm}/\mu\text{sec}$.

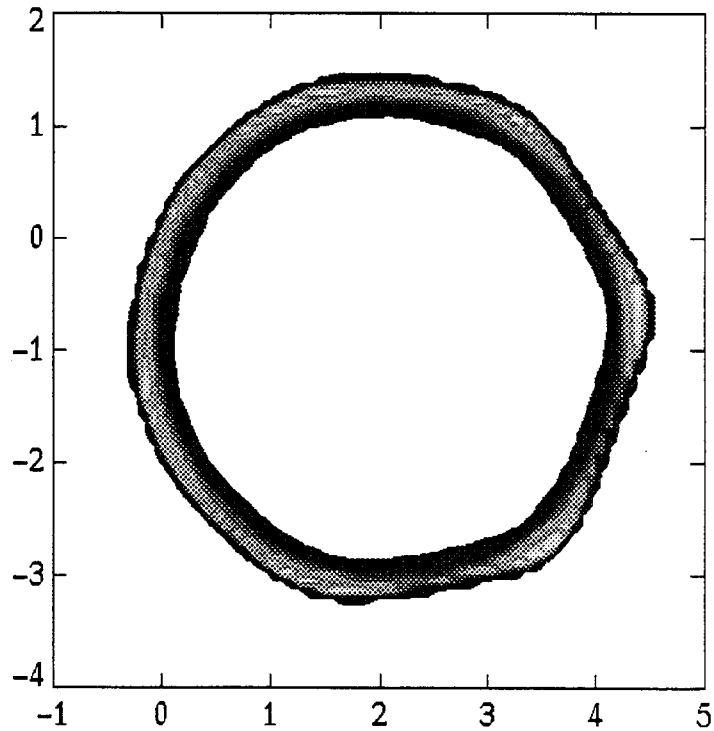


Figure 15. Imploding pinch with 2mm offset. Note asymmetry from initial post proximity.

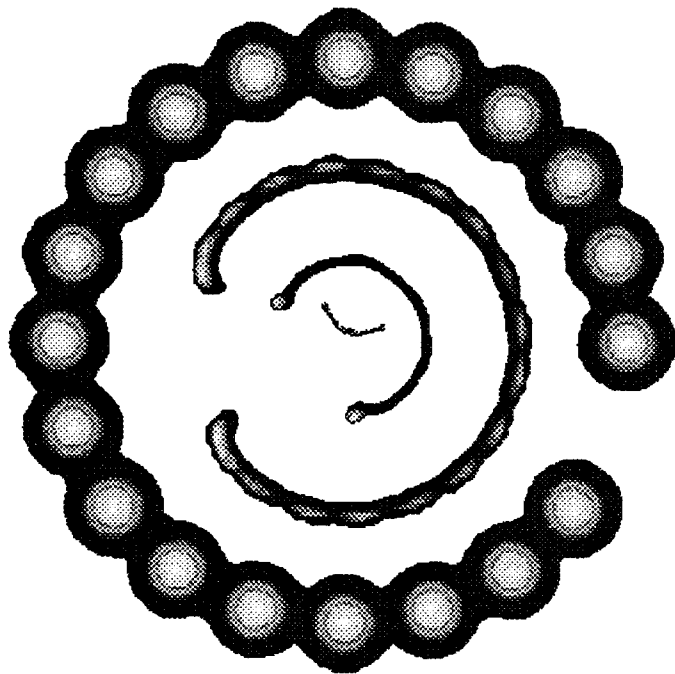


Figure 16. The 20 wire pinch with one wire missing. Initial average radius is 8.75 mm. The apparent rotation in this and Fig. 17 is a numerical artifact caused by random grid orientation.

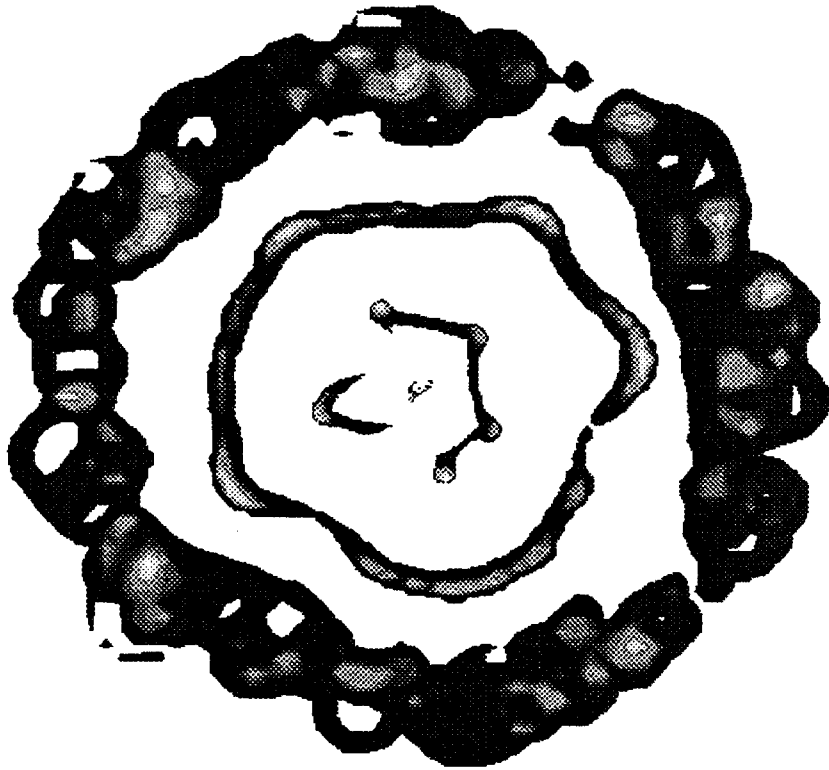


Figure 17. A 20 wire pinch with individual wires randomly displaced by 10% of their radius. Initial average radius is 8.75 mm.

The radiation power pulses for these four simulations, along with the infinite wire case, are shown in Fig. 18. Not surprisingly, large asymmetry or deviation from the uniform, motionless initialization results in reduced overall energy being radiated. The pulse has been lengthened to about 3 nsec in both the missing wire case and the random wire placement case, but not in the rotation or offset. The asymmetries in these numerical examples are larger than would normally be expected experimentally. If, however, the breaking of the current path does produce 3-D behavior, perhaps asymmetries of this magnitude could be produced. One case was studied experimentally, albeit inadvertently. Significantly reduced power output (~75%) was observed when a single wire in a 90-wire array broke and did not participate in the pinch [13,14].

The code has been used to examine possible radiation pulse broadening mechanisms involving other physical mechanisms. None have been found to be viable. The electric fields were found to be insufficient to produce significant numbers of runaway electrons [9]. Nor does a proposed (by Marder) "thermalization time" caused by ions passing through each other on axis due to their high temperatures and large relative velocities, seem to extend the pulse to anywhere near the amount observed. The conclusion, then, is that, aside from RT growth in the (r,z) plane, large asymmetry in the (x,y) plane is the only other mechanism found with the 2-D TIP code to broaden the sheath to values approximating the experiment. Just how important these asymmetries are, or if they are important at all in the experiments, is as yet unclear.

As always, it is important to remember that in all these (x,y) simulations, RT instabilities are expected to play a dominant role long before the radiation pulse is produced. The pulse width shown here is a numerical metric, not a physical prediction.

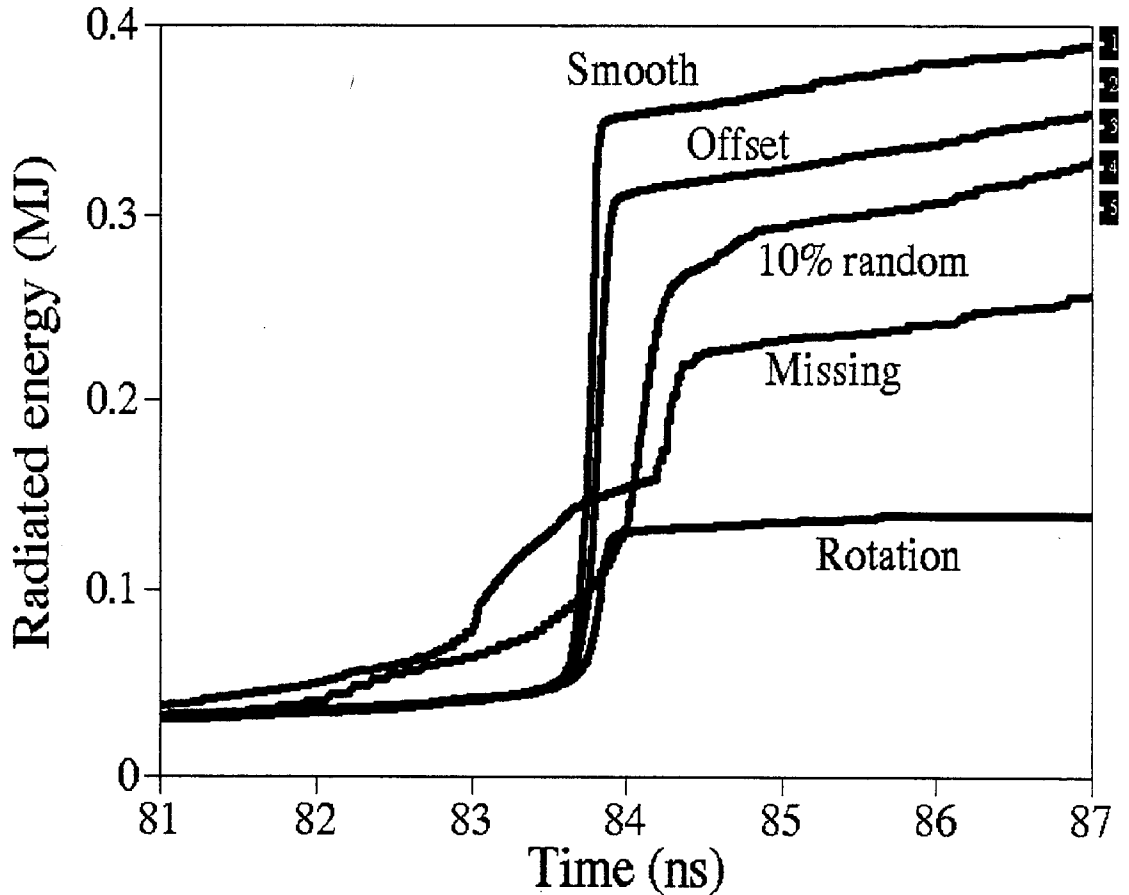


Figure 18. Power pulses from the asymmetric (x,y) simulations: Smooth, 2 mm offset, 10% random wire placement, 1 out of 20 wires missing, rotating pinch.

7. Conclusions.

By using TIP in different geometries to follow the behavior of a pinch formed from individual wires, the following observations can be made.

1. In contrast to the violent growth of instability in the (r,z) plane, the behavior in the (x,y) plane is quite benign. This contrast indicates that the z-pinch dynamics are dominated by RT instability growth.

2. For very sparse arrays, the wires can implode individually, never merging until essentially on axis. Increasing the wire number results in a continuous imploding plasma sheath. This qualitative difference could explain the sharp increase in radiated power as the number of wires passes 40. However, although the simulated radiated energy is somewhat lower with individual self-pinching wires than with a sheath, the radiation pulse duration remains very short.

Thus, the actual mechanism by which this qualitative difference manifests itself in a longer pulse must be found elsewhere, probably RT growth in (r,z) arising from 3-D effects in the explosion and merging of the individual wires [10]. Any asymmetry in the (x,y) plane degrades the performance, both in absolute radiated energy and the pulse width, although unless the asymmetries are large, the radiation pulse widths tend to be quite narrow.

3. The breaking of the current path caused by RT instability growth in two dimensions probably signals the onset of three dimensional behavior, although some 2-D codes can be made to continue running by allowing current to flow in very low density regions. If this 3-D behavior occurs, it could produce asymmetries analogous to the 2-D cases examined here and could thereby broaden the pulse width. Without firm evidence that these asymmetries actually occur, however, the hypothesis that the long (> 5 ns) radiation pulse widths are caused by RT broadening of the sheath remains unchallenged by anything in these studies.

A personal note.

So much of this work was made more relevant, productive, and enjoyable because George Allshouse was a collaborator on it. His untimely death earlier this year robbed us not only of a friend but of an invaluable source of physical insight, numerical savvy, and plain good sense. This paper is dedicated to his memory.

Appendix. A brief description of the TIP code.

Total Immersion PIC is a fluid particle in cell code in which "particles", representing fluid elements, carry virtually all the information. Particles are assigned mass, position, velocity, volume, internal energy, radiation energy, and either magnetic flux or vector potential. Quantities which are naturally advected, such as mass, energy, or magnetic flux, are simply carried by the moving particles. The grid is used to compute ensemble averages, such as density, and to solve elliptic diffusion equations. It is defined at each time step at a random location and (where applicable) orientation so as to extend just past the particles. Each particle transfers momentum and energy flux across grid boundaries in a manner appropriate to the current value of its thermodynamic variables. This accumulated flux is then redistributed to other particles in a strictly conservative manner. The elliptic equations required for heat conduction, radiation transport, and field diffusion are solved exactly using a block Thomas algorithm. While an exact solver may take a bit longer, it eliminates both the inaccuracy inherent in a fixed error bound or maximum number of iterations, and the possible (and, therefore, inevitable) failure of iterative schemes to converge. Spitzer resistivity and heat conduction are used, with the ionization and specific heat determined as a function of temperature from Mosher [11]. Rosseland and Planck opacities are found using density and temperature functional fits to XSN data. Radiation is a single energy group, flux-limited diffusion model. The plasma resistance and inductance are obtained from energy integrals. These, along with an external resistor, inductor, and voltage source are used in a total energy conservation equation to update the current at each time step. TIP exactly conserves mass, momentum, and energy in all three geometries.

A key feature of TIP is the artificial viscosity used to treat shocks, essentially the GAP [12] smoothing algorithm in which particle velocities are relaxed in a prescribed manner toward some average value. The subsequent decrease in kinetic energy is then returned to the particles as internal energy, simulating a true entropy-generating viscosity in a very intuitive way. The basic TIP philosophy is to include all relevant physical phenomena, but to use the simplest available approach to each. More details about the code are given in Appendix III of Ref. [9].

The most important numerical difference between the (r,z) and the other two versions is that the former solves for the magnetic field, B_θ , while the other two solve for the vector potential, A_z . To illustrate the functional equivalence of the three code versions when solving similar problems, Fig. 19 plots the radius versus time for five cases considered in this paper: the 1-D pinch (r,z) , the 2-D pinch in (r,z) , the smooth, infinite wire pinch in (x,y) , the 10 wire pinch in (x,y) and the 10 wire pinch in (r,θ) . As the figure indicates, when solving equivalent problems, the three versions give essentially equivalent results.

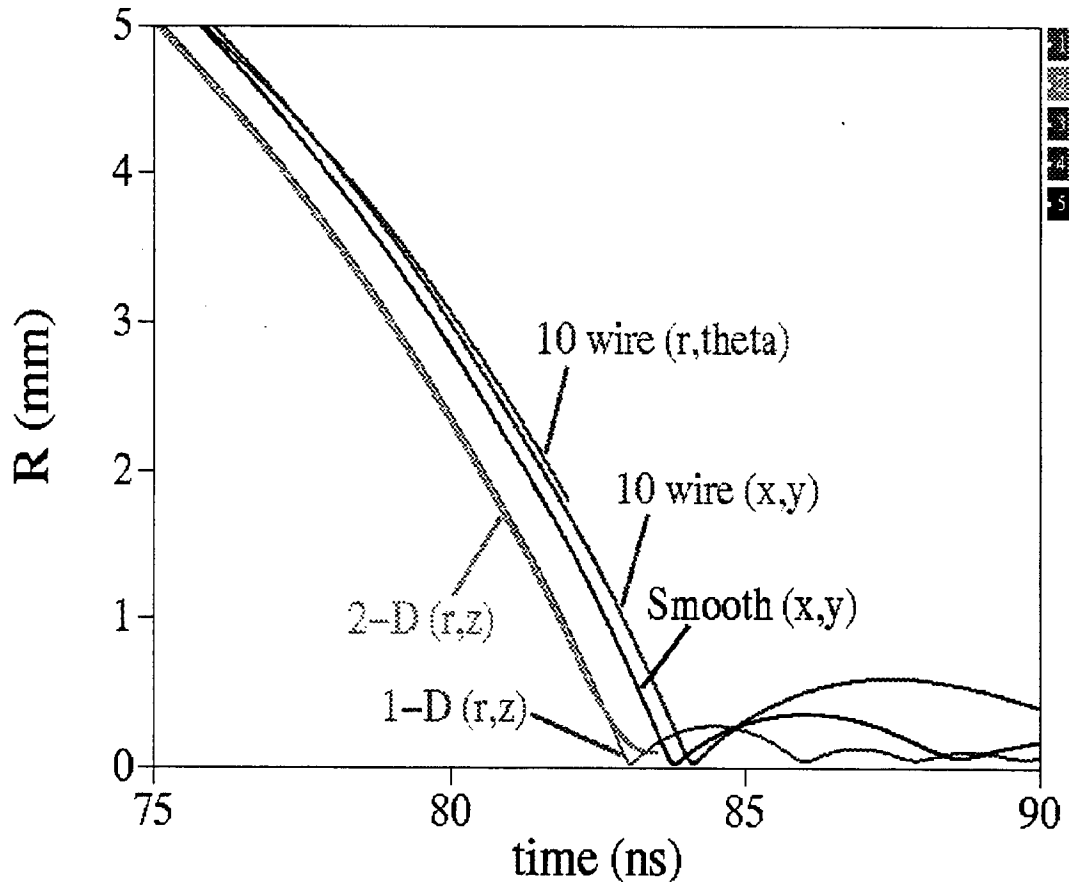


Figure 19. Radius versus time for equivalent runs in different geometries.

References.

- [1] T. W. L. Sanford, G. O. Allshouse, B. M. Marder, et al., "Improved symmetry greatly increases X-ray power from wire-array z-pinch", *Phys. Rev. Lett.*, **77**, 5063 (1996)
- [2] T. W. L. Sanford, D. L. Peterson, J.H. Hammer, et al., "Variation of high-power aluminum-wire array z-pinch dynamics with wire number, load mass, and array radius", Sandia National Laboratories Technical Report, SAND96-3031 (July, 1997) and to be published in Dense z-Pinches (4th International Conference, Vancouver, B.C., Canada, 1997), AIP Conf, Proc.
- [3] D.D. Bloomquist, et al., Proc. 6th Int. IEEE Pulsed Power Conf., Arlington, VA, (IEEE, N.Y., 1987), p310.
- [4] T.W.L. Sanford, J.H. Hammer, K.G. Whitney, et al., "Dynamics of a high-power aluminum-wire array z-pinch implosion" *Phys. Plasmas* **4**, 2188 (1997)
- [5] J.H. Hammer et al., "Two-dimensional radiation-magnetohydrodynamic simulations of Saturn imploding z-pinch", *Phys. Plasmas* **3**, 2063 (1996)
- [6] D.L. Peterson, et al., "Application of 2-D simulations to hollow z-pinch implosions" to be published in Dense z-Pinches (4th International Conference, Vancouver, B.C., Canada, 1997), AIP Conf, Proc.
- [7] M.R. Douglas, C. Deeney, N.F. Roderick, "Effect of sheath curvature on Reyleigh-Taylor mitigation in high-velocity uniform-fill, z-pinch implosions", *Phys. Rev. Lett*, **78**, 4577, (1997)
- [8] D. L. Peterson, et al., "Two-dimensional modeling of magnetically driven Rayleigh-Taylor instabilities in cylindrical Z pinches", *Phys. Plasmas* **3**, 368 (1995)
- [9] T.W.L. Sanford, D. Mosher, J.S. DeGroot, J.H. Hammer, B.M. Marder, et al., "X-ray emission from a high atomic number z-pinch plasma created from compact wire arrays" Sandia National Laboratories Technical Report, SAND96-0222 (March 1996)
- [10] D. Mosher, private communication.
- [11] D. Mosher, "Coronal equilibrium of high-atomic number plasmas", *Phys. Rev. A*, **10**, 2330 (1974)
- [12] B. M. Marder, "GAP - A PIC-Type fluid code", *Math. of Comp.*, **29**, 434 (1973)
- [13] T.W.L. Sanford, et al., "Dynamics of a high-power aluminum-wire array z-pinch implosion", *Phys. Plasmas* **4**, 2188 (1997)
- [14] K.G. Whitney, et al., "Analyzing time-resolved spectroscopic data from an azimuthally symmetric, aluminum-wire array, z-pinch implosion", *Phys. Rev. E*, **56**, 3540 (1997)

DISTRIBUTION:

- 2 University of New Mexico
Dept of Chemistry & Nucl Eng
Attn: Prof. G. Cooper
Prof. N.R. Roderick
Albuquerque, NM 87131
- 2 Los Alamos National Laboratory
Attn: R.J. Fehl
D.L. Peterson
P.O. Box 1663
Los Alamos, NM 87545
- 1 W.J. Schafer Assoc., Inc.
Attn: D.C. Straw
2000 Randolph Road SE, Suite 205
Albuquerque, NM 87106
- 2 Mission Research Corporation
Attn: D.R. Welch
K. Strive
1720 Randolph Road SE
Albuquerque, NM 87106
- 1 Titan Industries
Attn: R.B. Miller
P.O. Box 9254
Albuquerque, NM 87119
- 1 University of California Davis
Attn: Prof. John DeGroot
Dept. of Applied Science
228 Walker Hall
Davis, CA 95616
- 3 Harry Diamond Laboratories
Aurora Facility
Attn: J. Corrigan, Director
K.G. Kerris
J. McGarrity
2800 Powder Mill Road
Adelphi, MD 20783
- 11 Naval Research Laboratory
Attn: G. Cooperstein
D. Mosher
J.M. Neri
P. Ottinger
F.C. Young
R. Commisso
J. Davis
K.G. Whitney
J.P. Apruzese
P.E. Pulisifer
J.L. Giuliani
Washington, DC 20375
- 2 Cornell University
Laboratory of Plasma Sciences
Attn: Prof. J.B. Greenly
Prof. D.A. Hammer
369 Upson Hall
Ithica, NY 14853-7501
- 1 Massachusetts Institute of Technology
PLasma Fusion Center
Attn: Prof. R.D. Petrasso
167 Albany St.
Cambridge, MA 01239
- 1 University of Maryland
Laboratory for Plasma and Fusion Energy Studies
Attn: Prof. M. Reiser
College Park, MD 20742
- 1 Imperial College
Blackett Laboratory
Attn: Prof M. Haines
London SW7 2BZ
ENGLAND
- 2 Berkeley Research Associates
Attn: N.R. Pereira
J. Golden
P.O. Box 852
Springfield, VA 22150
- 3 Physics International Co.
Attn: C. Gilman
J.C. Riordan
P. Sincerny
2700 Merced Street
San Leandro, CA 94577
- 4 Pulse Science Inc.
Attn: V. Bailey
I. Smith
J. Fockler
P. Spence
600 McCormick Street
San Leandro, CA 94577
- 7 Lawrence Livermore National Laboratory
Attn: P.T. Springer
A. Toor
M.D. Rosen
M. Tabak
J.H. Hammer
G.B. Zimmerman
R.S. Thoe
P.O. Box 808
Livermore, CA 94550

1 Atomic Weapons Research Establishment
Attn: N. Fenner
Aldermaston, Reading RG7 4PR
Berkshire
ENGLAND

1 Weitzmann Institute
Department of Nuclear Physics
Attn: Y. Maron
Rehovot 76100
ISREAL

2 Kernforschungszentrum Karlsruhe GmbH.
Attn: W. Bauer
H. Bluhm
Postfach 3640, D-7500 Karlsruhe 1
GERMANY

1 Department of Energy
Attn: Kevin Bieg
DP-18
19901 Germantown Road
Germantown, MD xxxxx

1 MS 1393 D.L. Johnson, 5209
1 MS 0458 J.S. Rottler, 5607
1 MS 0151 G. Yonas, 9000
1 MS 0826 M.A. Cristen, 9111
1 MS 0819 J.S. Peery, 9231
1 MS 0819 A.C. Robinson, 9231
1 MS 0819 T.G. Trucano, 9231
1 MS 1170 G.A. Zawadzki, 9302
1 MS 1155 W. Beezhold, 9303
1 MS 1165 P.S. Raglin, 9304
1 MS 1178 J.J. Ramirez, 9310
1 MS 1159 M.A. Hedemann, 9311
1 MS 1179 W.P. Ballard, 9341
1 MS 1179 D.E. Beutler, 9341
1 MS 1179 J.A. Halbleib, 9341
1 MS 1179 R.P. Kensek, 9341
1 MS 1179 J.R. Lee, 9341
1 MS 1179 J.L. Lorence, 9341
1 MS 1179 T.F. Wrobel, 9341
1 MS 1106 R. Pepping, 9342
1 MS 1106 A.W. Sharpe, 9342
1 MS 1190 D.L. Cook, 9500
1 MS 1195 J.P. Quintenz, 9502
1 MS 1178 J.P. Corley, 9512
1 MS 1178 R. Hamil, 9512
1 MS 1182 D.D. Bloomquist, 9536
1 MS 1182 B.N. Turman, 9521
1 MS 1186 M.E. Cuneo, 9533
1 MS 1193 D.L. Hanson, 9531
1 MS 1193 D.J. Johnson, 9531
1 MS 1193 J.E. Maenchen, 9531
1 MS 1193 R.C. Mock, 9531
1 MS 1193 T.J. Renk, 9531
1 MS 1193 D.C. Rovang, 9531
1 MS 1186 M.P. Desjarlais, 9533
1 MS 1186 D. V. ... 9533

1 MS 1187 T.A. Mehlhorn, 9533
1 MS 1187 S.A. Slutz, 9533
1 MS 1184 J. Boyes, 9539
1 MS 1187 C.L. Olson, 9541
1 MS 1187 D.B. Seidel, 9542
1 MS 1187 M.R. Douglas, 9571
1 MS 1187 T.A. Hail, 9571
10 MS 1187 B.M. Marder, 9571
1 MS 1187 M.K. Matzen, 9571
1 MS 1187 E. McGuire, 9571
1 MS 1187 R. Olson, 9571
1 MS 1194 C. Deeney, 9573
1 MS 1194 T. Gilliland, 9573
1 MS 1194 D. Jobe, 9573
1 MS 1194 D.H. McDaniel, 9573
1 MS 1194 J. McGurn, 9573
1 MS 1194 T. Nash, 9573
1 MS 1194 J. Porter, 9573
1 MS 1194 S.E. Rosenthal, 9573
1 MS 1194 L. Ruggles, 9573
1 MS 1194 J. Seamen, 9573
1 MS 1194 R.B. Spielman, 9573
1 MS 1194 K. Struve, 9573
1 MS 1194 M. Vargas, 9573
1 MS 1196 G. Chandler, 9577
1 MS 1196 M. Derzon, 9577
1 MS 1196 D.H. Fehl, 9577
1 MS 1196 D. Hebron, 9577
1 MS 1196 R.J. Leeper, 9577
1 MS 1196 A.R. Moats, 9577
1 MS 1196 P. Reyes, 9577
1 MS 1196 C.L. Ruiz, 9577
10 MS 1193 T.W.L. Sanford, 9577
1 MS 1196 A. Schmidlapp, 9577
1 MS 1196 M. Stark, 9577
1 MS 1196 W.A. Stygar, 9577
1 MS 1196 J.A. Torres, 9577
1 MS 1196 J.T. Wagoner, 9577
5 MS 0899 Technical Library, 4916
2 MS 0619 Review & Approval Desk, 12690
For DOE/OSTI
1 MS 9018 CTF, 8940-2